Research Article

Venkata S. Reddy Channu*, B. Rambabu, Kusum Kumari, Rajmohan R. Kalluru, and Rudolf Holze

SnO_2/PANI nanocomposite electrodes for supercapacitors and lithium ion batteries

https://doi.org/10.1515/eetech-2018-0004
Received Nov 19, 2017; accepted Apr 05, 2018

Abstract: Tin oxide (SnO_2) nanostructures and SnO_2/Polyaniline (PANI) nanocomposites to be used as electrode materials for a lithium ion battery were synthesized using a solution-route technique with chelating agents followed by calcination at 300°C for 4 h. Structural and morphological properties were studied with powder X-ray diffraction, scanning electron and transmission electron microscopy. Particles of 25–10 nm size are observed in the microscope images. TGA results showed that the PANI-modified SnO_2 nanoparticles exhibit higher thermal stability than the SnO_2 nanoparticles. Electrochemical properties of SnO_2 and SnO_2/PANI electrodes were examined in a lithium ion battery and a supercapacitor. The electrode of SnO_2/PANI shows higher specific capacity. The cell **with** SnO_2/PANI exhibits a specific capacity of 1450 mAh/g at C/10. Supercapacitor results indicate that the PANI-modified SnO_2 composite had a higher current with apparent cathodic and anodic peaks.

Keywords: Nanoparticles; Solution-route method; Nanocomposites; Lithium ion batteries

1 Introduction

Lithium ion batteries (LIBs) are considered as the most operational ways and capable candidates for applications in the era of electric vehicles (EVs) (both plugin vehicles (PEV) and hybrid electric vehicles (HEVs)) aiming at carbon dioxide emission reduction, the most important cause of global warming, and meeting the growing scarcity of fossil fuels [1–4]. Conversely, successful application of lithium-ion battery technology will depend mostly on safety, long cycle life, and low cost which are controlled by the various materials used in the batteries [5, 6]. Graphitic carbon is commonly used as a negative electrode in commercial LIBs but exhibits poor rate performance due to its low lithium diffusion coefficient and presents serious safety issues (lithium metal deposition) because of potential solid electrolyte interphase (SEI) film formation [7–10]. Therefore, advanced materials with superior safety and excellent rate capability are critical components for the next generation lithium batteries.

In recent years, inorganic-organic nanocomposites have turned into a most attractive subject of research because of their particular physical and chemical properties [11]. Semiconductor-polymer nanocomposites are a predominantly capable new field of development of advanced materials in science and technology. The properties of these nanocomposites are quite different from those of the component materials because of interfacial interactions between nanostructured semiconductors and polymers. The properties of these materials can easily be tuned for desired applications through the variation of particle size, shape and distribution of nanoparticles.

Polypyrrole, polyaniline, and polythiophene were optional for applications as active electrode materials in primary and secondary batteries and in supercapacitors [12–14]. Among these polymers, polyaniline has attracted consideration because of its environmental stability, good electrical conductivity and easy synthesis [15]. A synergistic effect in polyaniline–inorganic nanocomposites, particularly in polyaniline–metal oxide composites, has been applied in electrode materials for supercapacitors and

***Corresponding Author: Venkata S. Reddy Channu:** SMC Corporation, College Station, TX 77845, United States of America; Email: chinares02@gmail.com; Tel: +12254853134
B. Rambabu: Solid State Ionics and Surface Sciences Lab, Department of Physics, Southern University and A&M College, Baton Rouge, LA 70813, United States of America
Kusum Kumari: Department of Physics, National Institute of Technology, Warangal, India
Rajmohan R. Kalluru: The University of Southern Mississippi, College of Science and Technology, 730 E Beach Blvd, Long Beach, MS 39560, United States of America
Rudolf Holze: Institut für Chemie, AG Elektrochemie, Technische Universität Chemnitz, D-09107 Chemnitz, Germany

lithium ion batteries. SnO_2 has the benefit of its environmentally benign nature and low cost. It is necessary to prepare and investigate composites combining excellent properties of both PANI and SnO_2 for electrochemical applications [16].

Several methods were reported in the literature for the synthesis of PANI-inorganic composite powders and thin films, for example, *ex-situ* intercalation process, drop cast method and *in-situ* self-assembly, hydrothermal and co-precipitation method [17–21]. However, to synthesize bulk amounts of fine particles of organic-inorganic powders requires low temperature and short duration of synthesis. The solution co-precipitation method is suitable to synthesize nanosize PANI-SnO_2 particles [21]. The present work reports on the synthesis of PANI-SnO_2 nanoparticles by a co-precipitation method using oxalic acid as a chelating agent.

2 Experimental

2.1 Synthesis of SnO_2 nanoparticles

0.1 M of oxalic acid (purity ≥ 99.0%, Sigma Aldrich) and 0.1 M of tin chloride ($SnCl_2 \cdot 2H_2O$) (purity ≥ 99.99%, Sigma Aldrich) were dissolved in 250 mL of distilled water under mixing with a magnetic stirrer for 4 h. Hydrogen peroxide (H_2O_2) (30 wt.% in H_2O, ACS reagent, Sigma Aldrich) was added to the above solution to oxidize tin ions into tin oxide, and the solution turns into a white-colored suspension of SnO_2. The suspension was aged at 90°C for 48 h. The white precipitate was filtrated and washed with a large amount of water and ethanol (purity 200 proof, Sigma Aldrich). It was dried at 100°C for 8 h and then calcinated at 300°C for 4 h.

2.2 Synthesis of polyaniline-modified SnO_2 nanoparticles

The white-colored suspension of SnO_2 was prepared using the solution route technique described above. It was mixed with 0.1 M aniline and kept below 4°C in an ice bath. After 30 min, 0.125 M of ammonium persulfate (APS) solution was added to the mixture, the ice bath was removed after a green-colored solution was obtained. The reactant mixture was stirred for 22 h and subsequently aged at 90°C for 48 h. The green precipitate was filtrated and washed with large amounts of water and acetone. It was dried at 100°C for 8 h and then calcinated at 300°C for 4 h. A color change from green to brown was observed after calcination.

2.3 Characterization

The crystallographic information of the samples was obtained using an X-ray powder diffractometer STADI P (STOE) with Ge(111) monochromatized Cu Kα radiation (λ = 1.54187 Å). Diffraction data were collected over the 2θ range from 10° to 80°. The morphologies of the resulting products were characterized using a scanning electron microscope (NanoNova SEM of FEI) and transmission electron microscopy (Philips CMG 200 FEG) (TEM). For TGA measurements a TA 600, operating in dynamic mode (heating rate = 10°C/min) was employed.

Electrochemical properties of SnO_2 nanoparticles were analyzed using a three-electrode cell with a platinum counter electrode and a silver wire in a solution saturated with KCl as the reference electrode. The working electrode, prepared by mixing 80 wt% of active material, 15 wt% of acetylene black and 5 wt% of polyvinylidene fluoride (PVDF), was coated onto a glassy carbon electrode with a diameter of 5 mm. An aqueous 2.0 mol/L solution of H_2SO_4 was used as the electrolyte. Cyclic voltammetric (CV) measurements were carried out between the potential limits of - 0.5 and 1.0 V against Ag/AgCl using a custom-built potentiostat. CV curves were recorded at $dE/dt = 10\ mV \cdot s^{-1}$.

The electrodes for cycling tests were prepared by mixing active material 75 wt.% with 15 wt.% acetylene black and 10 wt.% polyvinylidene fluoride (PVDF) binder in *N*-methyl-2-pyrrolidone (NMP). The mixture was coated on a stainless steel mesh, cut into 1-cm-diameter circular discs and kept at 100°C over night under vacuum. The dried electrodes were pressed by applying 0.5 tons of pressure. Typical electrode mass and thickness were 5 to 10 mg and 0.04 to 0.08 mm. The total mass of amorphous carbon and acetylene black used in SnO_2 and SnO_2/PANI electrode is 10 wt% in order to eliminate the impact of the conducting agent. The electrolyte was 1 M $LiPF_6$ in a mixture of ethylene carbonate (EC) and dimethyl carbonate (DMC) (1:1 by volume, Merck). Coin cells were fabricated in an argon-filled glove bag and with lithium foli as counter and reference electrode galvanostatically cycled with a current density 100 mA/g within a voltage range 0.0 . . . 3.0 V vs. Li/Li^+ with a Wuhan Land CT 2001A cycler at 25°C.

3 Results and discussion

Supercapacitors

Thermogravimetric analysis curves of SnO_2 and polyaniline-modified SnO_2 precursor are shown in Figure 1. The weight losses happened in three steps with SnO_2. The first weight loss was 0.06 mg in the temperature range 30 - 260°C; this weight loss could be attributed to evaporation of water on the surface of the SnO_2 and decomposition of the oxalic acid. The second and third weight losses of 0.48 mg and 3.25 mg in the temperature range 260 - 355°C and 355-400°C are attributed to decomposition of the tin chloride. The respective first weight loss was 0.45 mg in polyaniline-modified SnO_2 in the temperature range 30 - 110°C. This first weight loss corresponds to evaporation of water from the metal oxides. The second weight loss was 1.71 mg inpolyaniline-modified SnO_2 in the temperature range 110 - 620°C. This second weight loss can be attributed to decomposition of oxalic acid and polyaniline.

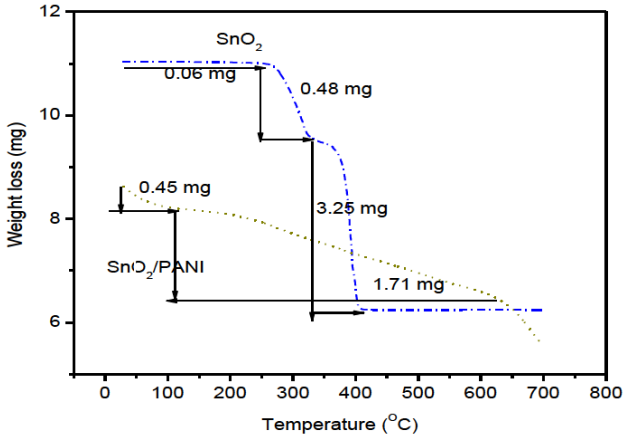

Figure 1: TGA curves of SnO_2 and SnO_2/PANI nanostructures.

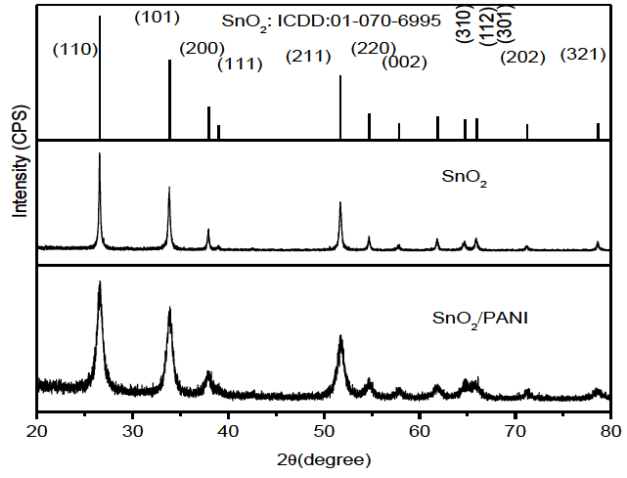

Figure 2: XRD patterns of SnO_2 and SnO_2/PANI nanostructures.

Figure 2 shows the XRD patterns of nanoparticles, data on phase purity and crystallographic information on the SnO_2 and polyaniline–modified SnO_2 nanoparticles were obtained using powder X-ray diffraction. All diffraction patterns of SnO_2 and polyaniline–modified SnO_2 nanoparticles show characteristic peaks of the tetragonal rutile phase. The XRD patterns are in good agreement with the standard data of the tetragonal rutile phase with a = 4.741 Å and c = 3.182 Å as the standard data file (ICDD

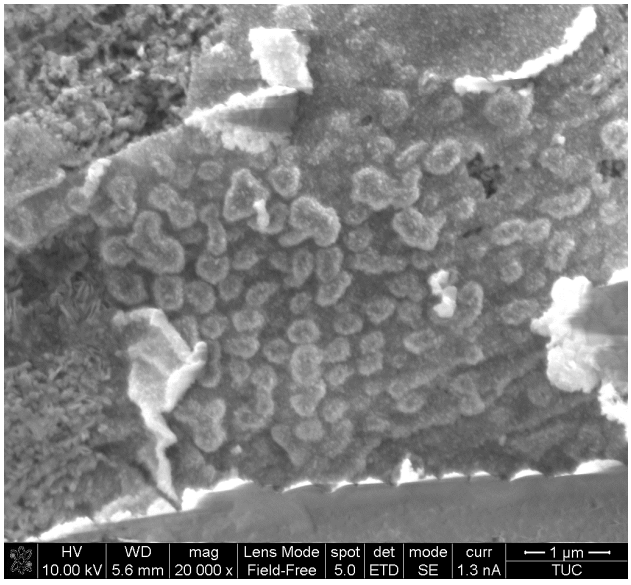

Figure 3a: SEM image of SnO_2 nanostructures.

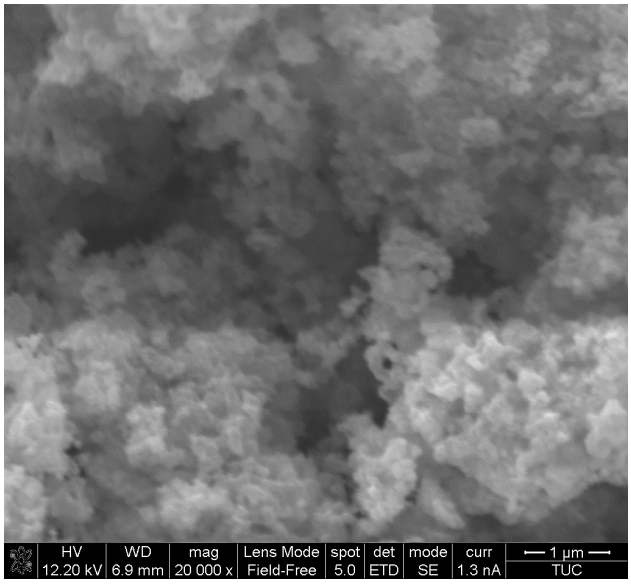

Figure 3b: SEM image of SnO_2/PANI nanostructures.

01-070-6995). No impurity phases were observed. The observed broadening of diffraction peaks in polyaniline–modified SnO_2 indicates incorporation of polyaniline in tin oxide [22].

The d-spacing of the SnO_2 and SnO_2/PANI nanostructures were estimated using the Scherrer formula [$\tau = K\lambda/\beta\cos\theta$] where τ is the mean size of the ordered domains, which may be smaller or equal to the grain size;

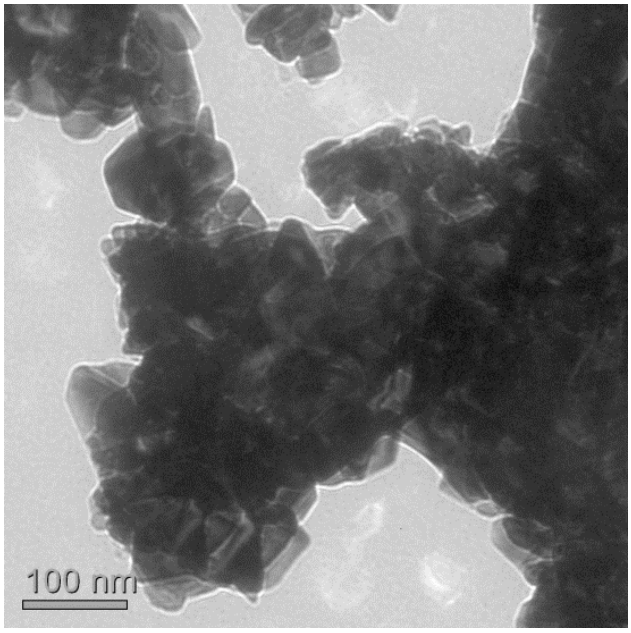

Figure 4a: TEM image of SnO_2 nanostructures.

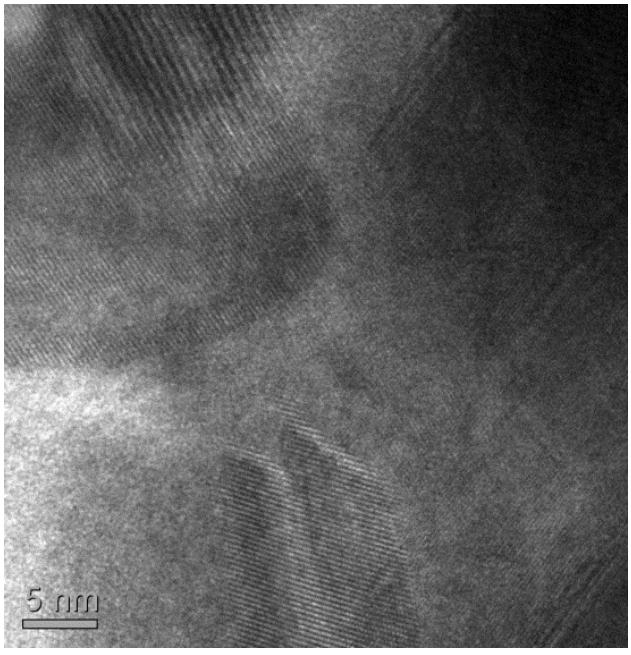

Figure 4b: HRTEM image of SnO_2 nanostructures.

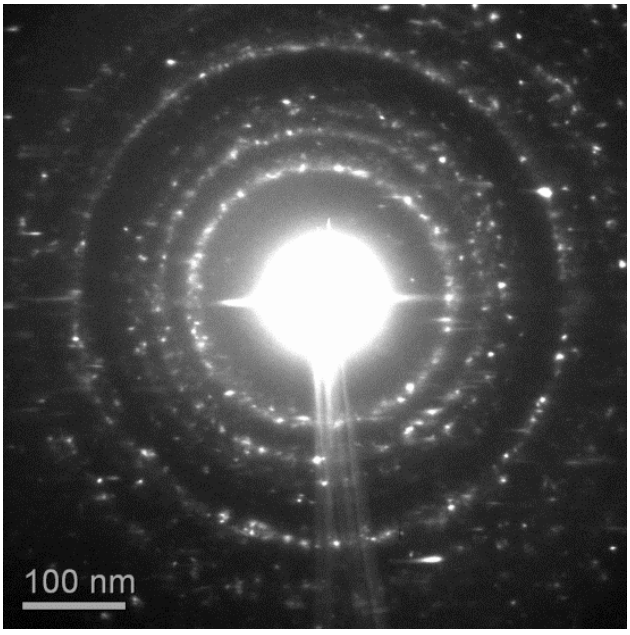

Figure 4c: SAED image of SnO_2 nanostructures.

K is a dimensionless shape factor, with a value close to unity (0.89). λ is the X-ray wavelength (1.54 Å); β is the line broadening at half maximum intensity (FWHM), after subtracting the instrumental line broadening, in radians. This quantity is also sometimes denoted as $\Delta(2\theta)$; θ is the Bragg angle. The calculated d-spacing is 4.9 Åfor SnO_2 and 5.9 Åfor SnO_2/PANI. The observed broadening of diffraction peaks in polyaniline-modified SnO_2 indicates incorpora-

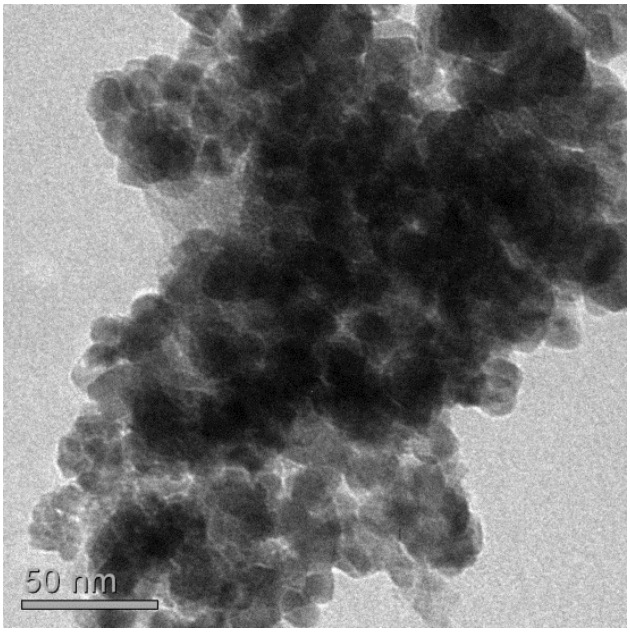

Figure 5a: TEM image of SnO_2/PANI nanostructures.

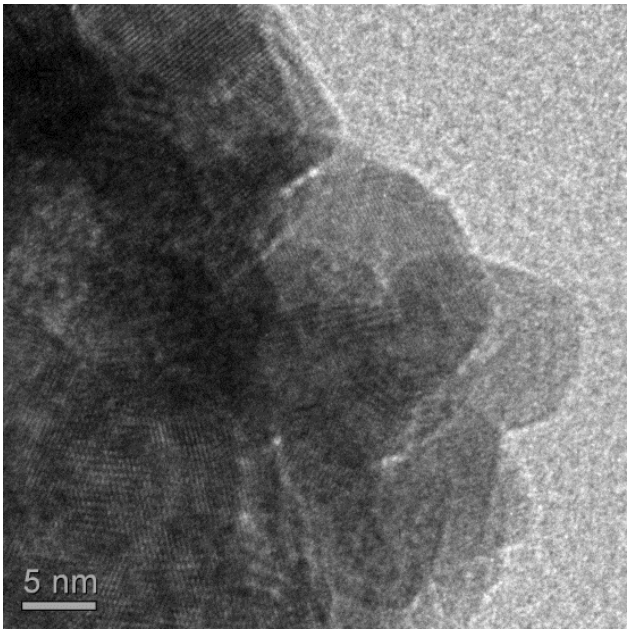

Figure 5b: HRTEM image of SnO_2/PANI nanostructures.

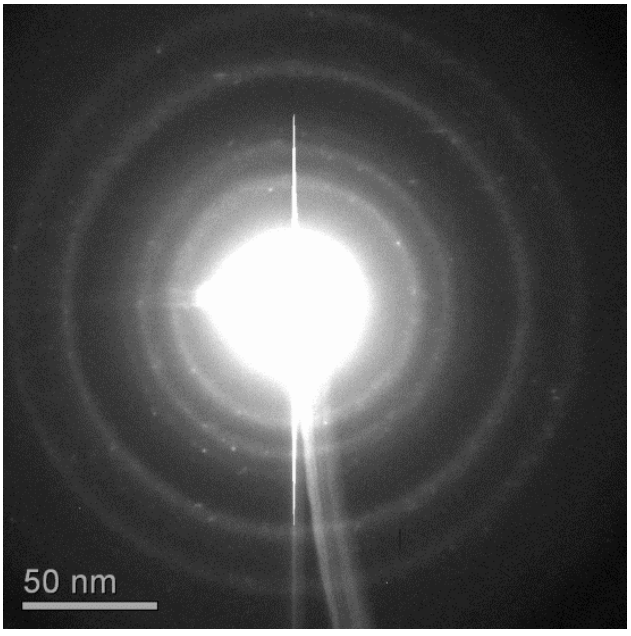

Figure 5c: SAED image of SnO_2/PANI nanostructures.

tion of polyaniline in tin oxide as the interlayer spacing increases from

4.9 Å to 5. 9 Å in SnO_2/ PANI nanocomposite. Obviously an exchange reaction has occurred between the proton/tin ion and the aniline molecule. It is more likely that the exchange involved the protonated form of aniline.

The SEM images indicate the formation of nanosized particles of SnO_2 and SnO_2/PANI (Figure 3a and Figure 3b).

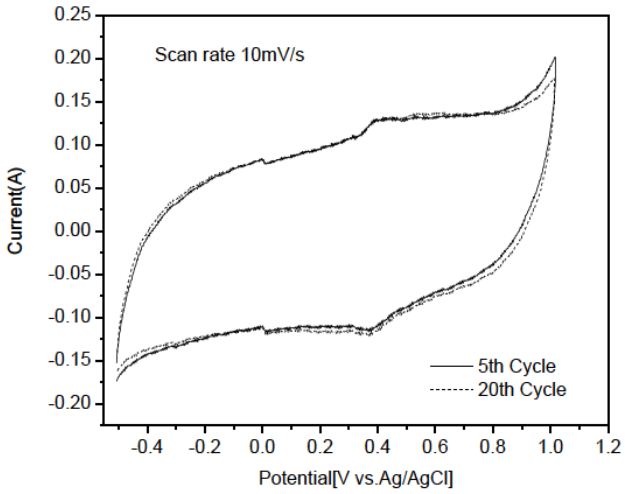

Figure 6a: Cyclic voltammogram of SnO_2 nanostructures.

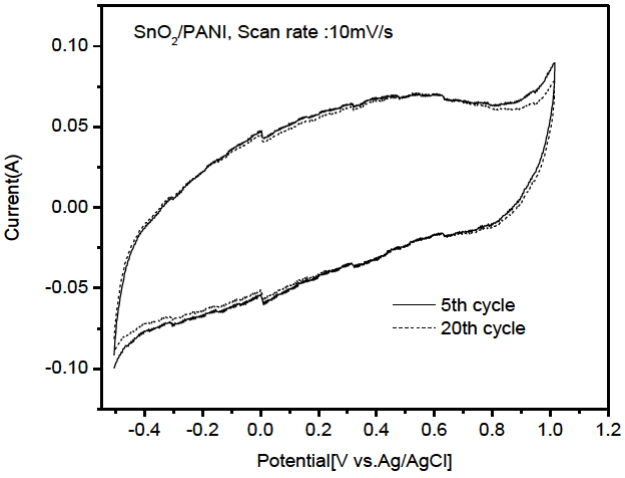

Figure 6b: Cyclic voltammogram of SnO_2/PANI nanostructures.

The transmission electron microscopy image of SnO_2 (Figure 4a) shows nanoparticles with 50 nm diameter. The high magnification HRTEM image clearly exhibits crystallinity (Figure 4b).The internal structure reveals particle growth along (111) direction. A typical selected area electron diffraction (SAED) pattern of a single nanoparticle is shown in Figure 4c. The diffraction spots can be indexed to a tetragonal rutile structure of SnO_2.

Figure 5a-5c show the TEM micrographs of the morphology, lattice image, and selected area diffraction pattern of the SnO_2/PANI. When comparing Figure 4a and 5a, we can observe that both materials have particle sizes about 50 nm in diameter. Figure 5b reveals that an incomplete thin carbon coating (approximately 5–10 nm thick) has been formed by the carbonization of organic matter that coated every crystallite yielding a SnO_2/PANI composite.

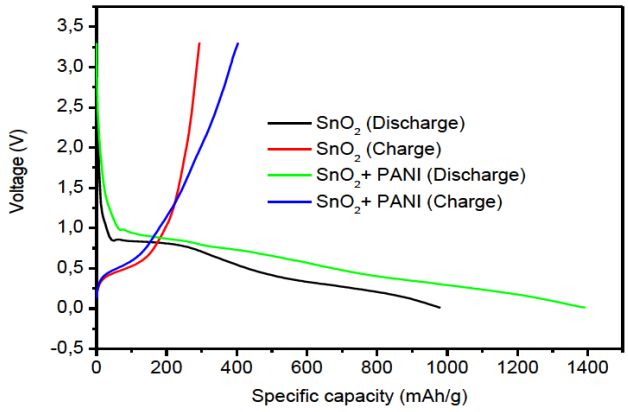

Figure 7a: Discharge curve of lithium ion battery electrodes within a potential window of 1.0–3.25 V vs. Li/Li^+.

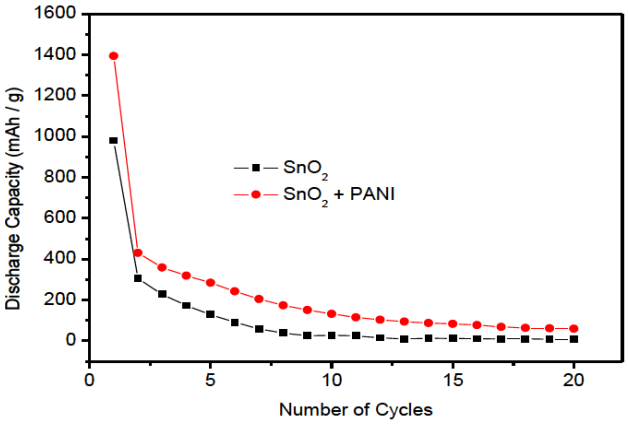

Figure 7b: Cycling performance of lithium ion battery electrodees.

The capacitance behavior of SnO_2 and PANI-modified SnO_2-nanoparticles as electrode materials has been studied using 2 M H_2SO_4 electrolyte solution within a potential window of - 0.5 to 1.0 V vs Ag/AgCl by cyclic voltammetry. Cyclic voltammograms of SnO_2 nanoparticles and PANI-modified SnO_2 nanoparticles are shown in Figure 6a and Figure 6b. The CV curves are more or less rectangular in shape within the measured potential window, indicating good charge propagation within the electrode due to acetylene black and a well-developed porosity. Anodic and cathodic peaks are observed in CVs of SnO_2 nanoparticles.

The CV of the PANI-modified SnO_2-nanocomposite (Figure 6b) presents a pseudocapacitive background current, but it also reveals visible current peaks. The ideal capacitor performance requires that redox processes occur continuously (causing pseudocapacitive behavior). Negative to 0.20 V PANI is in its entirely neutral state, designated as leucomeraldine (LE). At 0.20 V, LE undergoes partial oxidation resulting in the emeraldine (EM) state. If the potential becomes more positive, EM undergoes further oxidation yielding pernigraniline (PE). The oxidation and reduction processes are accompanied by ingress/egress of counter anions. Since these processes are reversible, charge storage in PANI provides a pseudocapacitive performance [8]. The shape of curves (Figure 6b) reveals that the capacitance feature of the PANI-modified SnO_2 nanocomposite electrode is mainly related to the redox mechanism. In Figure 6b, two processes of the PANI redox transitions are clearly observed. The anodic and cathodic peaks correspond to the LE/EM transition. Similarly, the anodic and cathodic peaks are attributed to the EM/PE transition. The occurrence of current peaks (albeit weak ones) is due to a very wide polydispersicity of PANI possiblycausing a very broad, almost disappearing peak. Apparently PANI as prepared here does not show this extreme distribution, instead a chain length correlated with the peak positions dominates resulting in the observed behavior.

Lithium Ion Battery Characterization

Galvanostatic discharge–charge profiles for the SnO_2 and SnO_2/PANI electrodes at 0.1 C current rates within a potential window of 0.0–3.25 V are shown in Figure 7a. The initial open-circuit voltage was 3.25 V. The curve related to the lithiation process does not have any plateaus that usually reflect phase formation or transition. The onset of the cathodic process seems to be at a potential below 1.5 V vs Li/Li+. The electrodes exhibit a reversible discharge capacity of 1000 mA h/g for SnO_2 and 1400 mAh/g for SnO_2/PANI. Compared to the pristine SnO_2 electrode, SnO_2/PANI electrode exhibits higher specific capacities; this may be due to a thin carbon layer deposition on the SnO_2, and also due to conducting polyaniline.

The cycling performance of SnO_2 and SnO_2/PANI is presented in Figure 7b. The cycling profiles clearly indicate the excellent performance of SnO_2/PANI at 0.1C current rate from 5^{th} to 20^{th} cycles.

4 Conclusions

SnO_2 and SnO_2/PANI have been synthesized through a simple solution-technique method with chelating agent. The solution-technique method is more economical in the large scale production of low-dimensional nanostructured SnO_2 and SnO_2/PANI. Electrochemical measurements indicate that the anode material SnO_2/PANI displays a highly reversible capacity. The obtained results

show that SnO_2 and SnO_2/PANI are highly promising anode material for electrochemical application.

Acknowledgement: One of the authors (V.S. Reddy Channu) thanks the Alexander von Humboldt Foundation for a fellowship for the period of 2010-2012.

References

[1] Tarascon J. M. and Armand M., Nature, 2001, 414, 359.
[2] Schiermeier Q., Tollefson J., Scully T., Witze A. and Morton O., Nature, 2008, 454,816.
[3] Yang S. B., Feng X. L. and Müllen K., Adv. Mater., 2011,23, 3575.
[4] Recham N., Chotard J. N., Dupont L., Delacourt C., Walker W., Armand M. and Tarascon J. M., Nat. Mater., 2010, 9, 68.
[5] Manthiram A., J. Phys. Chem. Lett., 2011, 2, 176.
[6] Shen L., Yuan C., Luo H., Zhang X., Xu K. and Zhang F. J., J. Mater. Chem., 2011, 21, 761.
[7] Guo B. K., Wang X. Q., Fulvio P. F., Chi M. F., Mahurin S. M., Sun X. G. and Dai S., Adv. Mater., 2011, 23,4661.
[8] Harpale K. V., Koiry S.P., Patil K. R., Aswal D. K., More M. A., J. Appl. Polym. Sci., 2015, 132, 41401.
[9] Chen Z. H., Qin Y., Ren Y., Lu W. Q., Orendorff C., Roth E. P. and Amine K., Energy Environ. Sci., 2011, 4, 4023.
[10] Amine K., Belharouak I., Chen Z. H., Tran T., Yumoto H., Ota N., Myung S. T. and Sun Y. K., Adv. Mater., 2010, 22,3052.
[11] Zhong-Ai H., Yu-Long X., Yao-Xian W., Li-Ping M., Yu-Ying Y., Zi-Yu Z., Mater Chem Phys., 2009, 114,990.
[12] Liang H.C., Chen F., Li R.G., Wang L., Deng Z.H., Electrochim Acta, 2004, 49,3463.
[13] Aurian-Blajeni B., Beebe X., Rauh R.D., Rose T.L., Electrochim Acta, 1989, 34,795.
[14] Kim Y.T., Tadai K., Mitani T., J Mater Chem., 2005, 15,4914.
[15] Christina O. B., Xin W. H., Wyatt N., Richard B. K., Chem. Soc. Rev., 2017,46, 1510.
[16] Zhang Q., Gao Q., Wei W.Q., Zhang H., Yanli T., Weiqian T., Zeyu L., Hong X., J. Mater. Chem. A, 2017, 5, 19136.
[17] Ma X., Wang M., Li G., Chen H., Bai R., Mater. Chem. Phys., 2006, 98, 241.
[18] Ram M. K., Yavuz O., Lahsangah V., Aldissi M., Sens Actuators B, 2005, 106,750
[19] Huiling T., Yadong J., Guangzhong X., Junsheng Y., J Mater Sci Technol., 2010, 26, 605.
[20] Lina G., Yingqiang Z., Xueliang H., Shurong W., Shoumin Z., Shihua W., Sens Actuators B., 2007,120, 568.
[21] Dutta K., De S.K., Materials Letters, 2007,61,4967.
[22] Deshpande N.G., Gudage Y.G., Ramphal S., Vyas J.C., Kim J.B., Lee Y.P., Sens Actuators B., 2009, 138,76.